Journal of Solid State Chemistry **164,** 88–97 (2002)
doi:10.1006/jssc.2001.9451, available online at http://www.idealibrary.com on IDEAL®

Modeling High-Energy Ball Milling in the Alumina–Yttria System

J. Alkebro,*,†,[1] S. Bégin-Colin,† A. Mocellin,† and R. Warren‡

*Division of Engineering Materials, Luleå University of Technology, SE-971 87 Luleå, Sweden; †Laboratoire de Science et Génie des Matériaux Métalliques, Ecole des Mines de Nancy, Parc de Saurupt, F-54042 Nancy Cedex, France; and ‡Department of Technology and Society, Malmö University, SE-205 06 Malmö, Sweden

Received July 25, 2001; in revised form October 25, 2001; accepted November 12, 2001

Experimental results from high-energy ball milling of alumina–yttria powder mixtures have been analyzed with models collected from the literature. Depending on the milling conditions, either there is formation of an intermediate phase in the alumina–yttria system (yttrium aluminum perovskite, YAP), or the sample becomes mostly amorphous. Variations due to milling tool material can be accounted for by local models based on the Hertzian theory of elastic bodies, but the effects of changing mills are poorly accounted for by published models. Therefore, the concept of an impact frequency distribution over the energy spectrum is introduced as a tool for studying the characteristics of the mills. The pressure on the powder trapped between two colliding bodies has been found to be the factor deciding the outcome of the process. The threshold behavior of the system yields an amorphous structure for low pressures, and formation of YAP when impact pressures exceed the threshold value. © 2002 Elsevier Science (USA)

Key Words: **high-energy ball milling; planetary ball milling; mechanical alloying; modeling; alumina; yttria; yttrium aluminum perovskite; YAP.**

INTRODUCTION

High-energy ball milling has been used for processes such as mechanical alloying and mechanical milling for some time. Several elementary models have been published, but the process is not yet completely understood. In particular, published models have mainly been based on experimental results for metallic materials, and it is not clear to what extent the conclusions are valid for ceramic systems.

Earlier work on milling of the Al_2O_3–Y_2O_3 system in a planetary ball mill (1, 2) has shown that, depending on the milling parameters, either the sample is amorphized or an intermediate phase (3, 4) of the system, $YAlO_3$ (YAP), is formed. This article aims to clarify what determines the final result of the process, and refine the published models for milling in a planetary ball mill.

[1]To whom correspondence should be addressed. Telefax: + 46-(0)920-49 10 84. E-mail: jesper.alkebro@mb.luth.se.

Modeling attempts have fallen mostly into the categories global models, concerned with the velocities and impact energies of the balls in the mill, and local models, discussing the mechanics of a single impact. Published work used to examine our experimental results is presented briefly below.

Global Models

Burgio *et al.* (5) as well as Abdellaoui and Gaffet (6) have discussed the simplified situation of a single ball in a planetary ball mill. As the vial rotates, the ball is pressed against the wall, which it follows without slipping or rolling. At a certain point, which we will call the take-off point, the forces on the ball change direction, throwing it across the vial with the flight velocity,

$$v_{\text{flight}} = \sqrt{(r_{\text{plate}}\Omega)^2 + (r_{\text{eff}}\omega)^2\left(1 - \frac{2\omega}{\Omega}\right)},$$

relative to the exterior of the mill. The parameters are defined in Table 1. Subsequently, the vial continues its orbit, while the linear movement of the ball eventually leads to a collision with the vial wall. At this point, the ball is considered to stick to the wall without rebounding, and then follow the movement of the vial until it again reaches the take-off point. Burgio *et al.* proposed an approximate analytical solution, but the trajectory can quite easily be calculated numerically. Abdellaoui and Gaffet considered the impact frequency for one ball to be

$$f = \frac{1}{t_{\text{flight}} + t_{\text{wall}}},$$

where t_{flight} is the time of flight, and t_{wall} is the time the ball is in contact with the wall before the next take-off.

During collision the impact energy, which under the current assumptions can be considered equivalent to the kinetic energy, is transferred to the powder. However, the impact energy is not the only factor determining the result of the

0022-4596/02 $35.00

TABLE 1
Characteristics of the Mills Used

Mill	Rotational speed (rad/s)		Radius (mm)						
	Central plate, Ω	Vials, ω	Central plate, r_{plate}	Vials, r_{vial}	Balls, r_{balls}	r_{eff}	Height (mm) of vials, h_{vial}	Number of balls	Ball mass (g)
P5	− 37.7	47.1	135	40	10	30	85	15	33
P7	− 74.4	74.4	75	20	7.5	12.5	40	7	14/6.2

Note. Rotational speeds are given in a fixed reference (as seen from outside the mill). The radius of the central plate refers to the distance from the center of rotation to the center of the vials, and r_{eff} designates the effective radius, i.e., r_{vial}-r_{balls}. Ball weights are for steel (33 g and 14 g) and alumina (6.2 g).

process. There have been several attempts to define quantities that will predict the outcome taking the pertinent parameters into account. Abdellaoui and Gaffet (6, 7) considered the total impact power divided by the mass of powder in the vial,

$$Q_{gp} = \frac{Efn_{balls}}{m_{powder}},$$

which we will refer to as the global power intensity, to be the important factor. Here, E is the impact energy, f the impact frequency for one ball, n_{balls} the number of balls in the vial, and m_{powder} the mass of powder in the vial. The correlation between the global power intensity and the result has also been studied by Bégin-Colin *et al.* (8).

It is known, however, that the behavior of a multiball system is not accurately described by the single ball simplification. Le Brun *et al.* (9) have photographed the interior of the vials during milling, showing that balls gather along the side in the vicinity of the departure point and that an "in-flight" ball goes through a tumbling movement over the others. Rather than uninterrupted flight through the vial, there is energy loss through a succession of collisions. In an attempt to account for these interactions, Burgio *et al.* (5) introduced the concept of a hindrance factor, which seeks to predict the remaining fraction of the single ball's energy. It is computed from the volume of the balls, and the wall surface covered by the balls. The corrected impact energy is then

$$E_{corr} = \varphi E,$$

where E is the impact energy with a single ball in the vial, and φ is the hindrance factor having a value between 0 and 1. In this way, Burgio *et al.* have successfully modeled the experimental results from varying sizes and numbers of balls in one mill.

Local Models

The global intensity parameters described above account for the mill used and its settings, but for milling with a constant powder to ball weight ratio (R), they predict the same result regardless of milling material. Experimental results have shown that this is not always true (2, 8), and so the mechanical properties of the milling tools must also be taken into account. Starting with the impact velocity calculated from the global models, local models consider the interaction between a ball, the powder, and the vial wall (or another ball), thus introducing the effects of milling tool material.

Several authors (10, 11) have calculated the pressure over a trapped volume of powder between colliding bodies using the Hertzian theory of elastic bodies. The contact area and the pressure distribution for a collision between clean surfaces has been assumed to remain essentially the same when a layer of powder covers the colliding surfaces. Even though elastic theory is used, the energy loss to the powder is usually considered to be complete, as would be the case for a plastic impact. Experiments observing the impact forces and the coefficient of restitution by Huang *et al.* (12) have shown that the thickness of the powder layer has an effect on both the transferred energy in one impact and the force upon the trapped volume. The energy transfer was seen to increase somewhat with a thicker layer of powder, whereas the maximum force decreased. Under the assumption that the Herzian contact area is constant, this leads to a decreasing maximum pressure on the trapped volume.

Hertzian contact theory predicts the radius of the trapped volume as well as the pressure on it while the amount of powder present in the vial decides the thickness of the powder layer. In the same spirit as above, milling parameters aiming to account for all the pertinent factors in the process have been proposed. Magini *et al.* (13) defined what we will refer to as the local energy intensity,

$$Q_{le} = \frac{E}{m_{trapped}},$$

where $m_{trapped}$ is the mass of trapped powder in an impact, and the energy E is taken from the global models. The mass of the trapped powder is determined by multiplying the

Hertz contact area by an estimated surface density of the powder. Bégin-Colin *et al.* (8) and Girot *et al.* (14) have considered the volume of trapped powder rather than the mass, but if the density of the powder is known, there is no difficulty in calculating one from the other. After an initial transient phase, the density of the powder should remain fairly constant during milling.

EXPERIMENTAL

Samples of two compositions have been prepared: mixture 1 containing 37.9 wt% alumina and 62.1 wt% yttria, and mixture 2 consisting of 21.9 wt% alumina and 78.1 wt% yttria. Most samples contained α-alumina (corundum) powder, but for comparison of reaction rates some were prepared using γ-alumina. They have been subjected to high-energy ball milling in two planetary ball mills, the Fritsch Pulverisette 7 (P7) using 7 balls and vials of either steel or alumina, or the Fritsch Pulverisette 5 (P5) using 15 steel balls. In the P7 the central plate rotated clockwise at 710 rpm, while the vials rotated counterclockwise at 710 rpm (as seen from outside the mill). The P5 rotated at 360 rpm and 450 rpm respectively. Powder to ball weight ratios (R) were 1/10, 1/20, or 1/40, and all milling experiments were performed continuously in air for times up to 8 h. The weight of the balls and the vials was measured before and after milling, thus giving an indication of the amount of contamination from the milling tools. After milling, the samples were examined by X-ray diffraction (XRD) using Co$K\alpha$ radiation ($\lambda = 0.1789$ nm), and electron microscopy (SEM). Before XRD the samples were mixed with 20 wt% Si powder as an internal standard. Peak areas obtained through a curve fit of selected undisturbed peaks of corundum YAP and Si have been used to determine the development of the corundum and YAP content in some of the samples. For corundum, the nonmilled sample served as reference, allowing for an absolute estimation, whereas the YAP content could only be determined relative to the other samples.

RESULTS

During milling the original cubic yttria structure was rapidly broken up and replaced by monoclinic yttria, which can be seen as a set of broad peaks in the XRD spectra (1). The α-alumina (corundum) structure was more resistant to milling and could still be detected after 8 h of milling. The XRD pattern of γ-alumina was initially diffuse, and disappeared completely during milling.

After these early stages, the samples evolved differently depending on milling parameters, which can be observed in Figs. 1 and 2. Three main results have been noted: (I) a mostly amorphous powder containing small amounts of crystalline alumina, (II) small amounts of YAP but otherwise like alternative I, and (III) most of the sample transformed into YAP. The content of YAP and corundum has been estimated from XRD data for some samples, as is shown in Fig. 3. Formation of YAP is simultaneous with the destruction of corundum, and when there is only amorphization the corundum content is generally higher. When using alumina tools, the contamination adds so much crystalline alumina that content estimates are no longer useful.

In most cases, changing R, but keeping all other parameters constant, only altered the milling time needed to obtain a given result. For example, with the P7 using steel tools, milling mixture 1 with $R = 1/20$ slightly more than twice as long as with $R = 1/40$, gave identical results in

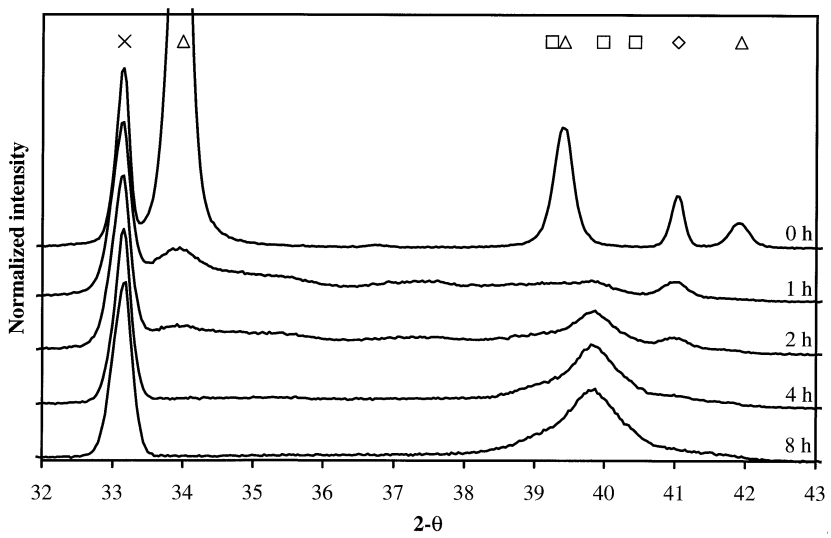

FIG. 1. XRD diagram of the development of mixture 1 during milling in P5 ($R = 1/20$). Si = ×, Y_2O_3 = △, Al_2O_3 = ◇, and $YAlO_3$ = □. The intensities of the Si peaks have been normalized.

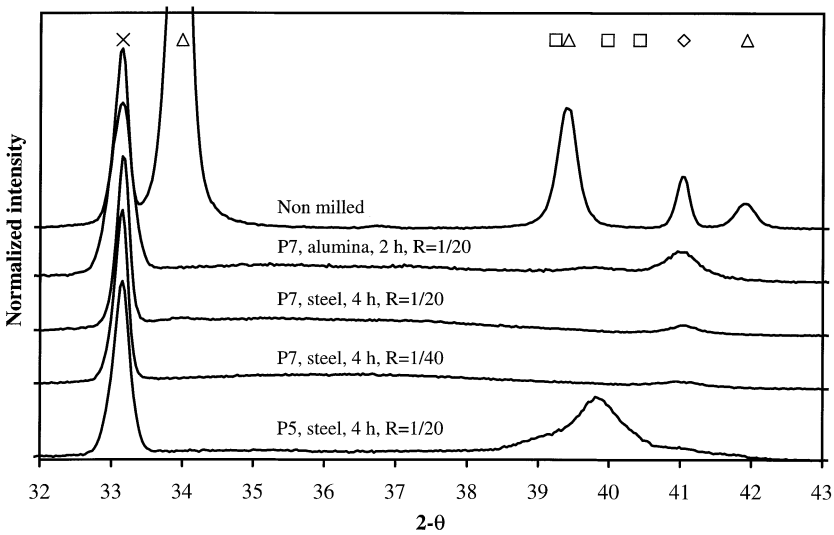

FIG. 2. The results after milling mixture 1 for 4 h in various mills, milling materials, and milling parameters. The intensities of the Si peaks have been normalized. Peak designations: Si = ×, Y_2O_3 = △, Al_2O_3 = ◇, and $YAlO_3$ = □.

XRD. However, when milling mixture 2 in this set-up, there was some formation of YAP for $R = 1/40$ but none observed for $R = 1/20$. Also in the P7 with steel tools, mixture 1 with γ-alumina formed YAP for $R = 1/40$, but the sample became completely amorphous for $R = 1/20$. It was thus seen that R had an effect, not only on the milling time required to reach a given stage of the process, but in some cases also on the final result.

Observations in SEM show that the smallest individual particles are in the range of 0.1 μm, but they form agglomerates of varying sizes from 1 μm to 10 μm. For powders milled in the P5 a layered structure was observed. After milling the powder was spread over the vial walls and could be scraped off with a spatula. Iron contamination was estimated from the weight loss of the milling tools to be typically between 5 and 10 wt% after 4 h of milling in both the P5 and the P7. Alumina contamination in the P7 was much greater, between 15 and 80 wt% after 4 h of milling. This severe contamination obscured the results of milling in analysis, but also altered R, thus changing the process itself. The level of contamination decreases with increasing R values.

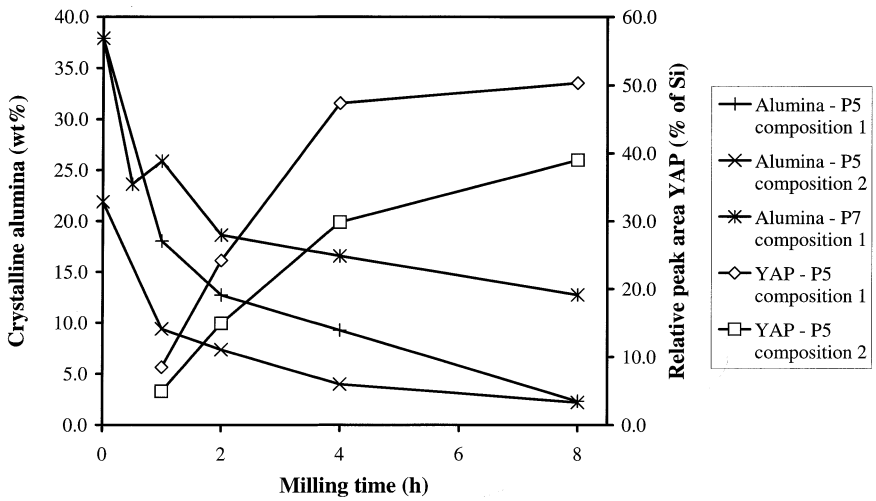

FIG. 3. Development of alumina and YAP contents for the P5 (steel tools, $R = 1/20$) and the P7 (steel tools, $R = 1/20$). For alumina the absolute content in the sample has been calculated using a nonmilled sample as reference. The YAP content is displayed as the relative peak areas YAP/Si of the integrated peaks. There was no YAP formed in the P7 sample.

The temperature during milling has not been measured, but the vials could be touched directly after milling. The vials in the P5 mill were somewhat warmer than those in the P7, but there was no difficulty in handling them. One sample of mixture 1 ($R = 1/20$) was milled in 15-min intervals followed by 45 min of cooling for a total milling time of 4 h in the P5. There was no difference in XRD between the sample milled in intervals and a sample milled continuously for 4 h.

DISCUSSION

Monoclinic yttria has 8% lower theoretical volume than cubic yttria (data from powder diffraction files), which favors the transformation to the monoclinic form under the high pressures created in the milling process. There have been several reports on monoclinic yttria formation under static high-pressure conditions such as 2.5 GPa at 550°C (15) or 1500°C (16), and 12 GPa at room temperature (17). Similarly, YAP has a lower theoretical volume than the corresponding amounts of alumina and yttria or alumina and YAG, which is favorable for YAP formation during milling. This is supported by Minkova and Tzvetkov (18), who have reported the transformation of YAG powder to alumina and YAP during high-energy milling.

Depending on milling conditions, formation of YAP or amorphization of the powder, and in some cases a combination of the two, are the final outcomes of the milling process. For a mill set-up that amorphizes the powder, there is no significant formation of YAP even if the milling time is extended. This is a typical sign of a threshold process (19, 20), as opposed to a cumulative process; i.e., it is not the accumulated energy of the impacts that governs the result but rather whether or not the energy of some impact is sufficient to bring the relevant milling parameter above a critical value. By analyzing the different cases in terms of the available models presented in the Introduction, the identification of the critical parameter should be possible.

As can be seen in Fig. 3, the destruction of corundum and the formation of YAP are related to each other. In samples where the corundum remains more intact, no reaction takes place and the final powder consists of amorphous material with residual corundum. Transition aluminas, such as γ-alumina, are typically less ordered and more reactive than corundum, and when used promote the formation of YAP where it otherwise would not form. When milled by itself, γ-alumina is reported to create corundum (21, 22), which has not been observed here. The reason may well be that the activation energy for formation of corundum is higher than for YAP. Zhang and Saito (23) report similar results from mechanochemical synthesis of $LaAlO_3$, with the reaction taking place for transition aluminas, but not for α-alumina.

By observing the rate of destruction of the corundum structure, the milling efficiency of the three mill set-ups (P7/steel tools, P7/alumina tools, and P5/steel tools) can be ranked. In view of the results in Fig. 3, the P5 with steel tools can be considered more efficient than the P7 with steel tools, which has also been reported by Guichard (24) for milling of $Al–Cr_2O_3$ mixtures. Contamination from the balls and vials impedes this comparison for the P7 using alumina tools, but the correlation between corundum destruction and YAP formation indirectly supplies the desired information: a higher content of YAP implies a more extensive destruction of corundum, thus enabling a ranking despite alumina contamination. Because there is some YAP formed in the P7 with alumina tools, it is considered more efficient than the P7 with steel tools. On the other hand, there is less YAP formation than in the P5. Thus, the three set-ups can be ranked in order of increasing efficiency as P7/steel tools, P7/alumina tools, P5/steel tools. The available models will now be examined with regard to their ability to predict this ranking.

Evaluation of Models

As mentioned in the Introduction, the global intensity parameters do not take the influence of milling materials into account. In Table 3 the global milling parameters for P7 can be seen to be identical regardless of milling material, even though experimental results show large differences (Table 2). Here, the mechanical properties of the milling tools and their influence on the impact must be considered using local models. Following the treatment of the Hertzian theory of elastic bodies by Timoshenko and Goodier (25), local parameters of a collision between a ball and a flat plate (representing the vial) have been calculated. The results, shown in Table 4, agree reasonably with the reported static pressures for the cubic to monoclinic transformation of yttria mentioned above. Calculated pressures exceed the elastic range of the milling tool material, but a recent

TABLE 2
Results of Milling under Different Conditions

Mill	Tools	R	Alumina type	Composition	Result
P7	Steel	1/40	α	1	Mostly amorphous
				2	Some YAP
			γ	1	Some YAP
		1/20	α	1	Mostly amorphous
				2	Mostly amorphous
			γ	1	Mostly amorphous
	Alumina	1/40	γ	1	Transformation to YAP
		1/20	γ	1	Transformation to YAP
			α	1	Some YAP
		1/10	γ	1	Transformation to YAP
P5	Steel	1/20	α	1	Transformation to YAP
			α	2	Transformation to YAP

TABLE 3
Global Model Parameters

	P7		P5,
	Steel tools	Alumina tools	Steel tools
Ball mass (g)	14	6.2	33
Flight velocity, v_{flight} (m/s)	5.8	5.8	5.7
Relative impact velocity, v_{relative} (m/s)	4.5	4.5	5.2
Impact energy, E (J)	0.14	0.06	0.44
Impact impulse, I_{impact} (kg m/s)	0.063	0.028	0.17
Impact frequency for single ball, f (Hz)	66	66	22
Impact power, P_{impact} (W)	65	29	147
Global power intensity (6, 7), Q_{gp}, for $R = 1/20$ (kW/kg)	13	13	6
Hindrance factor (5), φ	0.86	0.86	0.94

Note. The flight velocity, v_{flight}, has been used for calculating the trajectory of the ball and the impact frequency. All other impact parameters are computed using the relative impact velocity, v_{relative}.

publication (26) claims that in compression Hertzian theory formulas yield a good approximation even for plastic deformation. Also, the obtained pressures should be viewed as upper limit values since the powder will dampen the impact.

Assuming all the powder is evenly distributed on the walls of the vials, which is justified by the present experimental findings, the mass of trapped powder, m_{trapped}, is given by

$$m_{\text{trapped}} = \frac{m_{\text{powder}}}{2\pi r_{\text{vial}} h_{\text{vial}}} \pi r_{\text{contact}}^2 = \frac{m_{\text{powder}}}{2 r_{\text{vial}} h_{\text{vial}}} r_{\text{contact}}^2,$$

where m_{powder} is the total mass of the powder, r_{contact} is the Hertzian contact radius between the ball and the wall of the vial, and the other parameters are as defined in Table 1. This has been used when estimating the local energy intensity displayed in Table 4. The pressure on the trapped volume and the local energy intensity are both higher for alumina tools than for steel tools, which is consistent with the efficiency ranking above and the threshold nature of the YAP transformation.

TABLE 4
Local Model Parameters Calculated for a Ball Colliding with a Flat Plane

	P7		P5,
	Steel tools	Alumina tools	Steel tools
Relative impact velocity, v_{relative} (m/s)	4.5	4.5	5.2
Maximum pressure (25) (GPa)	6.3	8.6	6.7
Contact time (25) (μs)	39	23	50
Contact radius (25) (mm)	0.67	0.52	0.94
Local energy intensity (8), Q_{le}, for $R = 1/20$ (kJ/kg)	155	257	146

Note. Contact time, radius, and pressure have been calculated using Hertzian contact theory (25). The relative impact velocity, v_{relative}, has been used for all calculations.

In the P5, the central plate and vial motion are not the same as in the P7, and therefore the impact velocities will be different. Often, the flight velocity of the ball has simply been used when calculating local parameters, but the higher flight velocity of the P7 compared to the P5 (Table 3) would indicate higher pressures and local energy intensities for the P7, which is opposite to the experimental results. The movements of the balls must therefore be examined in greater detail. Consequently, a numerical calculation of the flight trajectories of a single ball has been performed.

During flight, the distance between the ball and the center of the vial can easily be expressed as a function of time. Solving the equation for when the ball strikes the wall, i.e., when the distance to the center of the vial equals the radius of the vial, gives the time of flight, and the motion of the ball within the vial can be plotted. The velocity of the ball is now known at every instant, and the impact frequency can be determined by adding the time of flight to the time in contact with the wall, as described in the Introduction.

When plotted as seen by a viewer positioned at the center of the plate and following its rotation, the take-off point is always in the same place and the ball seemingly follows a curved trajectory being accelerated by the centrifugal force. Such a plot can be seen in Fig. 4, and it is in good agreement with similar plots made by Schilz (27). The curved trajectory in this frame of reference shows that the velocity of the vial is not negligible compared to the flight velocity. Had this been the case, the ball trajectory would have been nearly a straight line in both frames of reference. Compared with the earlier mentioned approximate analytical solution by Burgio *et al.* (5), the numerical calculations allow a more exact estimation of the relative impact velocity, i.e., the velocity change of the ball during impact, which we define as

$$v_{\text{relative}} = |\bar{v}_{\text{pi}} - \bar{v}_{\text{flight}}|,$$

where v_{pi} is the velocity of the vial wall at the point of impact and v_{flight} the flight velocity, both in vector form. The calculated velocities and the resulting impact energies are given in Table 3.

Calculating the local parameters using the relative impact velocity (Table 4) is a beneficial modification, but hardly sufficient to explain the large difference in experimental results. The next measure in refining the model is to consider the interactions between balls in the mill. The tumbling movement of the balls photographed by Le Brun *et al.* (9) leads to energy loss as the ball travels through the vial. The

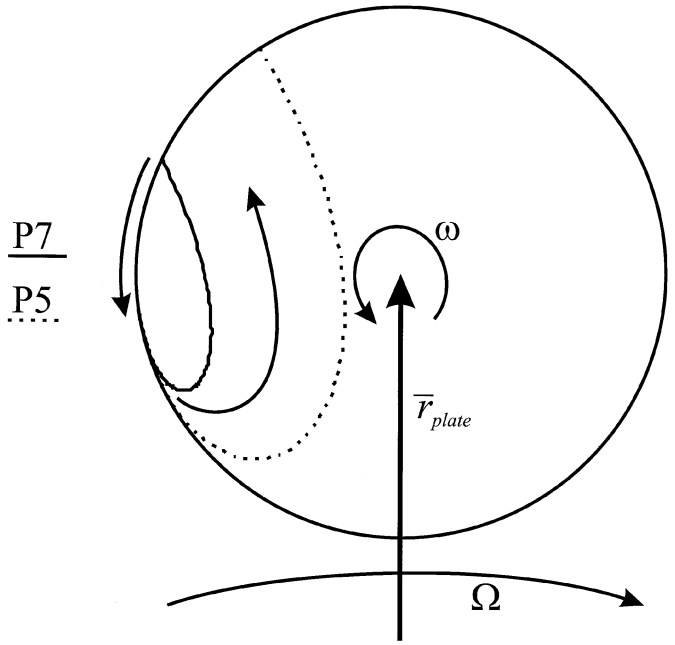

FIG. 4. Calculated ball trajectories for a single ball plotted as seen by an observer at the center of the plate following with the rotation, i.e., the frame of reference rotates clockwise with the rotational speed Ω. In this frame of reference, r_{plate} will not move and the take-off point will always be in the same place. The radius of the plots has been normalized.

hindrance factor defined by Burgio *et al.* (5, 19, 20) successfully describes this energy loss as a function of vial loading, but the calculated values displayed in Table 3 do not differ sufficiently to account for the effects of changing mills. These shortcomings of the published models in accounting for experimental results have led to a new approach to the interactions between balls within the mill, which will be described below.

Frequency Distribution of Impact Energies

In the reference system used in Fig. 4, as discussed above, the ball is accelerated all along its trajectory by the centrifugal force. Most of the relative impact velocity comes from this acceleration, so v_{relative} will increase with the undisturbed flight path. This means that the impact energy will be strongly dependent on the undisturbed flight path. It follows that the tumbling motion of the balls (9), which leads to shortened flight paths, will result in a large proportion of low-energy impacts. Girot *et al.* (28) have discussed the frequency of impact energy levels, finding that only a minority of impacts have enough energy to drive the process.

Given the random nature of the resulting trajectory and the large amount of impacts, it should be possible to describe the energy of the impacts statistically by a frequency distribution of impact energy, i.e., a function describing how often impacts of a certain energy occur. The demands on such a distribution would be that it predicts a large amount of low-energy impacts and few high-energy impacts. Furthermore, it should be easily normalized and adaptable to different mills.

An exponential function is common in physics for expressing energy distributions, and it complies with the demands above. Also, the calculation in Appendix A, based on the treatment by Reif (29), supports that choice. In its normalized form,

$$g(E) = k\ \mathrm{e}^{-kE},$$

where k is the distribution constant and E is the impact energy, it expresses the probability distribution of impact over the energy spectrum. The probability of an impact energy between energies E_1 and E_2 would be

$$\int_{E_1}^{E_2} g(E)\,dE = \int_{E_1}^{E_2} k\ \mathrm{e}^{-kE}\,dE.$$

If the impact frequency, all energies included, is C, the impact frequency in the interval E_1 to E_2 will be

$$f_{E_1-E_2} = \int_{E_1}^{E_2} Cg(E)\,dE = C\int_{E_1}^{E_2} k\ \mathrm{e}^{-kE}\,dE,$$

and the power of these impacts

$$P_{E_1-E_2} = \int_{E_1}^{E_2} CEg(E)\,dE = C\int_{E_1}^{E_2} Ek\ \mathrm{e}^{-kE}\,dE,$$

with the total power supplied to the system being

$$P_{\text{tot}} = C\int_0^{\infty} Ek\ \mathrm{e}^{-kE}\,dE = \frac{C}{k}.$$

The mathematical development above shows how the two parameters C and k control the process. This allows a reasonable fit to the results of Dallimore and McCormick (30, 31), as can be seen in Fig. 5.

There is no simple formula for calculating how the impact frequency C and the distribution parameter k change when going from the P5 to the P7, but some estimates can be made. In Fig. 4 the calculated trajectories for single balls predict that milling balls in the P5 will strive for a wider trajectory than in the P7. With most of the balls gathered along the side of the vial near the take-off point (9), a wider trajectory can be expected to decrease the risk of collision with other balls and give longer stretches of undisturbed flight. This leads to a lower value of the distribution factor k for the P5, which will result in a higher tail of the frequency distribution at high energies. The rotational speed of the plate and the vials is lower in the P5, and the impact

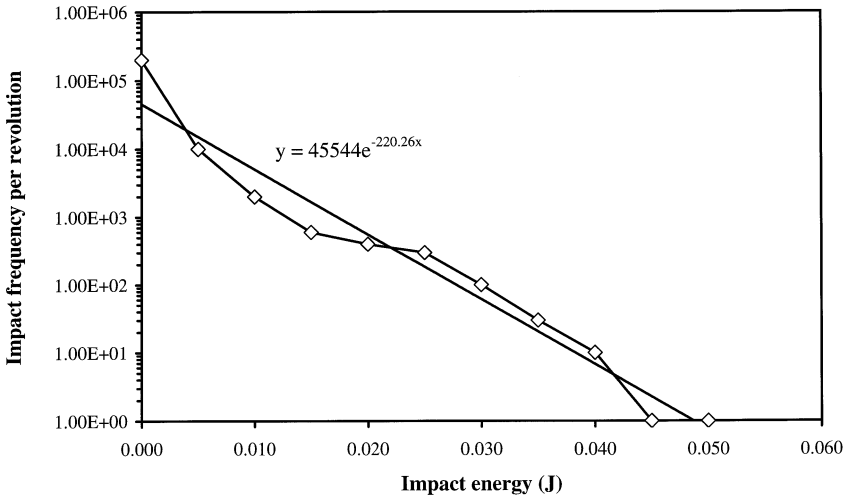

FIG. 5. Curve fit of the impact energy–frequency distribution to simulation data points for a P5 rotating at 330 rpm, taken from Dallimore and McCormick (30). This form of distribution can be made to fit reasonably with simulation results.

frequency C can thus be expected to be lower. However, given the threshold type of reaction of the sample, the change of the distribution of impact energies should be much more important than the change in impact frequency as such, which would explain the experimental results.

In practice, the parameters of the distribution would have to be determined for each set-up. Ideally this would be done by measuring the power input and the collision frequency of the mill. Iasonna and Magini (19) and Magini *et al.* (20) have shown that the power of the electric motor can be correlated to the milling power dispersed within the vials. Further information on the characteristics of a mill can be collected by milling systems with well-known thermodynamic properties. The kinetics and reaction products of threshold systems give information on both the power injected and the energy distribution of the shocks.

Pertinent Local Parameter

Local models are needed to determine the trapped volume and the pressures upon it, and these factors decide the threshold value of the impact energy for a system. For instance, for the set-ups in Table 1, the threshold impact energies are not the same since differences in ball material and diameter change pressures and contact areas. This leads to the hitherto unanswered question as to which local parameter governs the final result of the milling process.

When R is changed from 1/20 to 1/40 there will be half as much powder in the vial, which will halve the powder thickness. The energy transferred to the powder will decrease somewhat (12), and the Hertzian contact radius is expected to remain constant, or possibly increase very slightly. In all, this should nearly double the local energy intensity, Q_{1e}. In Table 4, the calculated local energy intensity for steel is roughly half the value for alumina for a given R. Even though the actual impact energies differ from the case of a single ball, impact velocities should be similar for the two materials, and thus the ratio of the local energy intensities remains as calculated. Combining the effects of the two parameters, steel milling tools should have about the same local energy intensity at $R = 1/40$ as alumina milling tools at $R = 1/20$. However, the differing experimental results lead us to the conclusion that the local energy intensity, Q_{1e}, is not the parameter governing the result of the process.

With a thicker powder layer, some of the impact energy is spent rearranging and sliding grains in the powder at the onset of impact (12). Less energy is available for the deformation of the grains, and the result is a lower maximum pressure on the trapped volume. As milling proceeds, the powder layer is more compacted along the walls of the vial and differences can be expected to diminish, but not disappear. The rather small variations of the maximum pressure expected from powder thickness are consistent with the vague effects observed experimentally; i.e., sometimes there is a difference in end products, but mostly not. When there is a difference, a thinner powder layer has been seen to coincide with the formation of YAP. Therefore, the maximum pressure upon the trapped volume seems to best correlate with the experimental results. The pressure is distributed unevenly through the volume, causing very high forces at some contact points, which in turn triggers the reaction. The relatively narrow peaks of the YAP suggest the possibility of crystallization through localized heating.

CONCLUSIONS

High-energy ball milling of alumina–yttria powder mixtures in a planetary ball mill is a threshold process in which the pressure upon the powder trapped in collisions is the

factor deciding the outcome. With sufficiently high pressures during impact, the system forms YAP ($YAlO_3$); otherwise the system goes toward an amorphous structure. Local models based on Hertzian contact theory account for differences in results when changing milling tool material, but available global models, based on the movement of a single ball in the vial, do not adequately explain the effects of using another mill. To better describe the observed experimental effects, we have introduced a frequency distribution of impact energies to account for energy loss due to interactions between balls in the vial. It allows the characteristics of the mill set-up to be described by two parameters, the impact frequency and the energy distribution factor. The distribution compares reasonably with published simulation data.

APPENDIX A

Let a ball have a constant acceleration a starting from zero velocity. A number of identical balls are considered to be motionless, randomly scattered in the path of the accelerated ball, and when a collision occurs with one of them all kinetic energy is lost. This is a simplification of the situation in the vial as seen in a rotating reference system such as in Fig. 4. The probability of impact in the time interval t to $t + dt$, $\rho(t)dt$, is considered to be proportional to the distance covered, which gives

$$\rho(t)\,dt = c_1 u(t)\,dt = c_1 at\,dt,$$

where c_1 is a constant and $u(t)$ is the velocity of the ball at time t. With $\Omega(t)$ being the probability of no collision up to the time t, the treatment by Reif (29) yields

$$\frac{1}{\Omega(t)}\frac{d\Omega(t)}{dt} = -\rho(t) = c_1 at,$$

which is solved by

$$\ln\Omega(t) = -\frac{1}{2}c_1 at^2 + c_2 \Rightarrow \Omega(t) = \exp\left(-\frac{c_1 a}{2}t^2\right),$$

where the constant $c_2 = 0$ since $\Omega(0) = 1$.

Now, the probability of avoiding a collision up to time t, and then having a collision between t and $t + dt$, is $\Omega(t)\rho(t)dt$, which defines the distribution of time between the impacts as

$$h(t) = \Omega(t)\rho(t) = c_1 at\exp\left(-\frac{c_1 a}{2}t^2\right).$$

The kinetic energy of the ball $E = 1/2m(at)^2$, where m is the mass of the ball, gives

$$t = \frac{1}{a}\sqrt{\frac{2E}{m}} \Rightarrow dt = \frac{1}{a\sqrt{2mE}}\,dE.$$

Knowing that $h(t)\,dt = g(E)\,dE$, we can now express the distribution of the impacts in the energy domain as

$$g(E)\,dE = \frac{c_1}{am}\exp\left(-\frac{c_1}{am}E\right)dE.$$

This finally gives us an energy distribution of the form

$$g(E) = k\,\mathrm{e}^{-kE},$$

where

$$k = \frac{c_1}{am}$$

is constant for a given mill set-up.

ACKNOWLEDGMENTS

This research was made possible by grants from the Swedish Research Council for Engineering Sciences (TFR) and the Faculty of Engineering at Luleå University of Technology.

REFERENCES

1. J. Alkebro, S. Bégin-Colin, A. Mocellin, and R. Warren, *J. Eur. Ceram. Soc.* **20,** 2169–2174 (2000).
2. J. Alkebro, R. Warren, S. Bégin-Colin, and A. Mocellin, *Ceram. Eng. Sci. Proc.* **21**(4), 87–94 (2000).
3. B. Cockayne, *J. Less-Common Metals* **114,** 199–206 (1985).
4. "Phase Diagrams for Ceramists, Vol. II" (E. M. Levin, C. R. Robbins, and H. F. McMurdie, Eds.), pp. 56–57. Am. Ceram. Soc., Columbus, OH, 1969.
5. N. Burgio, A. Iasonna, M. Magini, S. Martelli, and F. Padela, *Il Nuovo Cimento* **13D**(4), 459–476 (1991).
6. M. Abdellaoui and E. Gaffet, *Acta Metall. Mater.* **43**(3), 1087–1098 (1995).
7. M. Abdellaoui and E. Gaffet, *Mater. Sci. Forum* **179–181,** 339–344 (1995).
8. S. Bégin-Colin, T. Girot, G. Le Caër, and A. Mocellin, *J. Solid State Chem.* **149,** 41–48 (2000), doi:10.1006/jssc.1999.8491.
9. P. Le Brun, L. Froyen, and L. Delaey, *Mater. Sci. Eng. A* **161,** 75–82 (1993).
10. G. B. Schaffer and J. S. Forrester, *J. Mater. Sci.* **32,** 3157–3162 (1997).
11. D. R. Maurice and T. H. Courtney, *Metall. Trans. A* **21,** 289–303 (1990).
12. H. Huang, M. P. Dallimore, J. Pan, and P. G. McCormick, *Mater. Sci. Eng. A* **241,** 38–47 (1998).
13. M. Magini, A. Iasonna, and F. Padella, *Scr. Mater.* **34**(1), 13–19 (1996).
14. T. Girot, S. Bégin-Colin, X. Devaux, G. Le Caër, and A. Mocellin, accepted by *J. Mater. Synth. Proc.*

15. H. R. Hoekstra, *Inorg. Chem.* **5**(5), 754–757 (1966).
16. V. Srikanth, A. Sato, J. Yoshimoto, J. H. Kim, and T. Ikegami, *Cryst. Res. Tech.* **29**(7), 981–984 (1994).
17. E. Husson, C. Proust, P. Gillet, and J. P. Itié, *Mater. Res. Bull.* **34**(12–13), 2085–2092 (1999).
18. N. Minkova and G. Tzvetkov, *Mater. Lett.* **35,** 135–138 (1998).
19. A. Iasonna and M. Magini, *Acta Mater.* **44**(3), 1109–1117 (1996).
20. M. Magini, C. Colella, A. Iasonna, and F. Padella, *Acta Mater.* **46**(8), 2841–2850 (1998).
21. P. A. Zielinski, R. Schulz, S. Kaliaguine, and A. Van Neste, *J. Mater. Res.* **8**(11), 2985–2992 (1993).
22. A. Tonejc, C. Kosanovic, M. Stubicar, A. M. Tonejc, B. Subotic, and I. Smit, *J. Alloys Compds.* **204,** L1–L3 (1994).
23. Q. Zhang and F. Saito, *J. Am. Ceram. Soc.* **83**(2), 439–441 (2000).
24. J.-L. Guichard, Ph.D. thesis, Institut National Polytechnique de Lorraine, Nancy, France, 1998.
25. S. P. Timoshenko and J. N. Goodier, "Theory of Elasticity," pp. 409–422. McGraw-Hill, New York, NY, 1970.
26. D. Gugan, *Am. J. Phys.* **68**(11), 920–924 (2000).
27. J. Schilz, *Mater. Trans. JIM* **39**(11), 1152–1157 (1998).
28. T. Girot, X. Devaux, S. Bégin-Colin, G. Le Caër, and A. Mocellin, *Philos. Mag. A* **81**(2), 489–499 (2001).
29. F. Reif, "Fundamentals of Statistical and Thermal Physics," pp. 463–467. McGraw-Hill, Singapore, 1985.
30. M. P. Dallimore and P. G. McCormick, *Mater. Trans. JIM* **37**(5), 1091–1098 (1996).
31. M. P. Dallimore and P. G. McCormick, *Mater. Sci. Forum* **235–238,** 5–14 (1997).